JOURNAL OF MATERIALS SCIENCE 28 (1993) 1919–1936

Some factors influencing the formation of reaction-bonded silicon nitride

R. G. PIGEON, A. VARMA*, A. E. MILLER‡
Department of Chemical Engineering and ‡Department of Electrical Engineering, University of Notre Dame, Notre Dame, IN 46556, USA

Several salient factors influencing the formation of reaction-bonded silicon nitride (RBSN) compacts have been studied. These include the effects of mullite and alumina furnace tubes typically employed during "high-purity" nitridation studies, pre-sintering of green silicon compacts, free powder versus compact nitridation, and the influence of metal/metal oxide additions. The latter studies have provided experimental evidence for enhancement due to dissociated nitrogen, and suggest that (1) β-Si_3N_4 formation does not necessarily require a liquid phase, (2) atomic nitrogen stimulates β-phase formation, and (3) the liquid phase provides an efficient source for volatile silicon, promoting α-Si_3N_4. These conclusions are consistent with accepted mechanisms for the formation of the two phases.

1. Introduction

Formation of silicon nitride, Si_3N_4, through the reaction-bonding process is an economically attractive method for obtaining intricately shaped bodies of reasonable density (70%–90%) that can subsequently be post-densified to near theoretical values [1]. The most remarkable feature of the process is the retention of the overall external dimensions to within about 0.1% in transforming from a silicon compact to a partially densified silicon nitride body. Post-machining costs are significantly reduced, and a relatively high-volume throughput may be possible in an industrial environment.

The reaction-bonded silicon nitride (RBSN) process involves the formation of a green silicon compact by one of a variety of methods such as injection moulding, slip casting, or isostatic pressing. Pre-sintering may be used to achieve a body of sufficient integrity so that it may be conventionally machined to the required shape and tolerance, or alternatively, the sample may be directly nitrided without any pre-sintering. Nitridation is typically carried out in a nitrogen or nitrogen-containing atmosphere between the temperatures of 1200 and 1450 °C. Hydrogen, helium, or argon may be added to the nitriding gas in varying ratios to alter the concentration of nitrogen, to control the rate of development and the exothermicity of the reaction, and to change the thermal properties and molecular diffusivity of the gas. As the reaction proceeds, each of the individual grains of silicon expands by 21.8 vol% in transforming to Si_3N_4. This expansion is taken up into the interstitial space between the particles within the compact, resulting in the characteristic pore filling and density increase. Permeability decreases by more than three orders of magnitude [2], and hence, maintaining through porosity is one of the more difficult aspects of the process in the attempt to achieve full conversion in a reasonable amount of time. Ideally, there would be just the right amount and type of porosity so that full conversion would occur at the same instant when voids and porosity are completely eliminated. Unfortunately, this is unlikely to ever be realized in actual practice.

Reasonable success with densified RBSN has stimulated a renewed interest in its development [3–9], due to the high cost and difficulties associated with silicon nitride bodies produced by hot-isostatic pressing and pressure sintering of the ceramic powder. Owing to the high degree of covalent bonding [10], these latter methods require relatively large quantities (1–10 wt%) of oxide or non-oxide liquid-phase sintering additives, which tend to be detrimental to the high-temperature properties. Additionally, high linear shrinkage (15%–20%) renders the production of exact shapes rather difficult, so that extensive post-machining may be required, which often is the most expensive step in the manufacturing process. Post-densification of RBSN compacts is, of course, not completely void of these difficulties or its own inherent complications. However, owing to the relatively high starting densities of 2.2–2.8 g cm^{-3} that can be achieved with minimal additives (0–1 wt%), this method offers an attractive alternative to direct sintering of Si_3N_4 powder in the attempt to achieve a final product with good high-temperature properties.

Comparison of RBSN nitridation data from different laboratories is typically restricted to qualitative agreement, owing to a variety of factors influencing the process to varying degrees. Such factors include

* Author to whom all correspondence should be addressed.

0022–2461

the nitridation temperature [2, 11, 12], the sample heating profile [13, 14], particle shape and size distribution of the starting powder [2, 15], impurities present in the sample (either native or added) [16–25], impurities derived from external sources such as the nitriding atmosphere and the furnace tube [26, 27], composition of the nitriding atmosphere [28–41], pretreatment conditions [42], and whether the gas is static or flowing [43]. Much of the discrepancy in the published data can be attributed to the lack of control of one or more of these variables, either intentionally or by indiscretion.

In this light, we attempt to address a few salient factors in the reaction-bonding process that unfortunately render nitridation data tractable only to qualitative consideration, rather than allowing for quantitative kinetic analysis and support of mathematical models that would be applicable to all nitriding systems. The factors investigated include the ceramic furnace tube typically employed in "high-purity" nitridation studies, pre-sintering of green silicon compacts, free powder versus compact nitridation, and the influence of metal/metal oxide additions.

2. Experimental procedure

2.1. Apparatus

Kinetic studies in the nitridation of silicon are amenable to thermogravimetric analysis (TGA). During the reaction to form silicon nitride, the individual silicon particles experience a mass increase of 66.5% upon full conversion. This mass increase allows the progress of the reaction to be readily followed, yielding mass (i.e. per cent conversion) data as a continuous function of time if all weight differences observed by the TGA can be attributed to the formation of the nitride ceramic. Additionally, the TGA system readily allows for the continuous delivery of any desired nitriding gas mixture. A schematic diagram of the nitriding apparatus is shown in Fig. 1.

The nitridation kinetics described herein were obtained using a Cahn 2000 recording electrobalance (1.5 g capacity; 0.5 μg sensitivity) and a rapid heat/cool, Kanthal Super 33 split-shell furnace (Model 3320, Applied Test Systems, Inc., Butler, PA) controlled by a sealed Pt–Pt 10% Rh thermocouple placed directly below the sample. The electrobalance was encased in a gas-tight vacuum bottle to allow strict control of the nitriding atmosphere. Ultra-high-purity gases were passed through a static mixer, followed by an oxygen and water trap (OxiClear® gas purifier, Alltech Associates, Inc., Deerfield, IL) to ensure concentrations of less than 50 p.p.b. (5×10^{-8} atm), and then immediately delivered to the reactor. Analysis of the gas mixture was accomplished using a Carle 111 gas chromatograph for accurate determination of feed and exit stream compositions. A Beckman NO/NO_x analyser for determining the presence of oxides of nitrogen (NO, NO_2) down to the parts per million level was also available. The possible existence of nitrogen oxides provided a further check of whether or not even trace quantities of oxygen were present during nitridation.

The reactor itself was comprised of a 3/4 in (1.90 cm) i.d. high-purity alumina tube (McDanel Refractory Co., Beaver Falls, PA), lined along its inner surface with a 0.025 mm thick sheet of molybdenum (99.95%) foil to act as an oxygen getter, so that any residual oxygen left in the system prior to nitridation, or any oxygen released by or diffusing through the alumina tube, was gettered by the molybdenum at temperatures above 500 °C. Hence, the silicon samples were never allowed to be in proximity of potential oxygen sources. The molybdenum foil was also instrumental in blocking the flow of undesired species, such as SiO_2, SiO, and various volatile metallic impurities that would be expected to originate from the tube itself at high nitridation temperatures, and hence, could dramatically alter the observed kinetics.

2.2. Procedure

The desired amount of 99.999% silicon powder (-325 mesh (< 43 μm), Cerac, Inc., Milwaukee, WI), with a mean particle size of 4.2 μm and a BET area of 1.54 $m^2 g^{-1}$, was weighed into a molybdenum crucible (produced in-house using 0.025 mm molybdenum foil) (6 mm i.d. × 5 mm high), which was then attached to a single-crystal sapphire (250 μm diameter, Saphikon, Inc., Milford, NH) hangdown wire using a tungsten wire basket support. Sample size was chosen to minimize the effects of reaction exothermicity (748 kJ mol^{-1}) so that transient melting within the compact was not an issue, including samples impregnated with various metal additives. The samples were reacted isothermally at temperatures ranging between 1185 and 1350 °C in a typical gas mixture of 5% H_2/N_2 at 0.4 p.s.i.g. (10^3 p.s.i. = 6.89 N mm^{-2}). The gas mixture was admitted to the reactor at 150 $\pm$ 2 cm^3 min^{-1} only after extensive outgassing of the entire system was carried out.

The outgassing procedure for the silicon nitridation apparatus utilized a roughing pump in a repeated fashion, somewhat analogous to a batch extraction process. The system was pumped down to approximately 0.1 torr ($\simeq$13.3322 Pa) filled with the reacting gas mixture, and then pumped back down to 0.1 torr. The gas mixture was allowed to flow through the apparatus and equilibriate for several hours, only after the extraction process was repeated at least four times.

Once equilibrium was established, the furnace was heated at maximum controller output to 900 °C (which represents a temperature too low for any detectable reaction to occur) and then ramped in a linear profile up to the desired isothermal reaction temperature (1185–1370 °C) at a rate of 340 C h^{-1}. The 0–10 mV analogue output from the Cahn electrobalance was recorded on a strip-chart recorder (yielding a resolution of 0.01 mg) and also digitized on a Macintosh IIci computer running LabVIEW 2 software (National Instruments, Austin, TX).

Some of the silicon samples were nitrided directly, while others were impregnated with $ZrCl_4$ or the nitrate salts of either iron, calcium or chromium dissolved in spectroscopic-grade MeOH using an in-

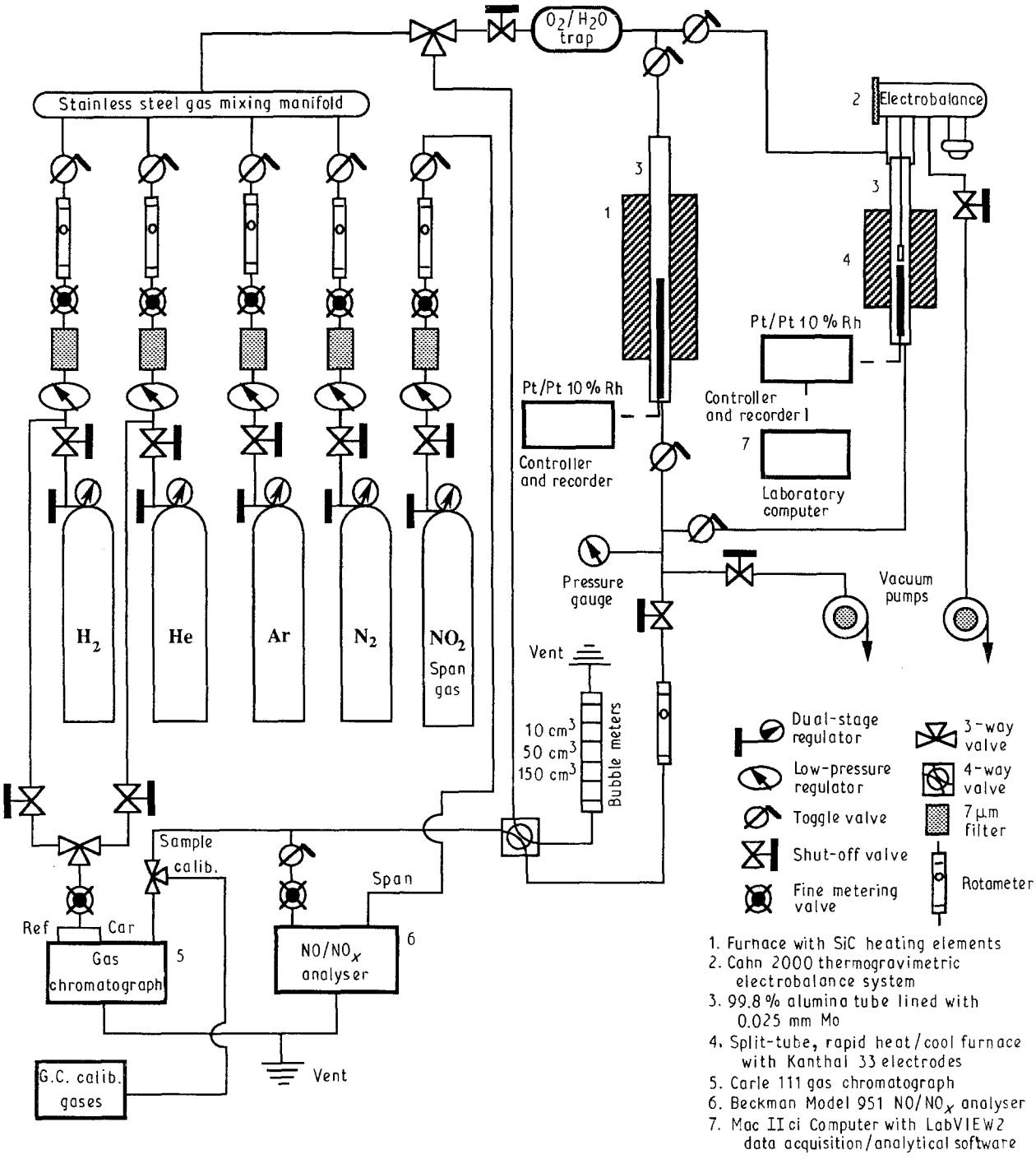

Figure 1 Schematic representation of the silicon nitridation apparatus.

cipient wetness deposition technique to yield high dispersion of the catalytic agents on the surface of the silicon particles. The incipient wetness volume (i.e. the minimum volume of solution required to fill the voids between the particles) was determined by micropipetting solvent liquid on to a 100 mg green sample. An incipient volume of 43 μl was determined for this sample size (consistent with the calculated void fraction) by the first observance of a tacky consistency on the surface of the green body. The samples were subsequently air dried at room temperature for 1–2 h or until weight changes were no longer observed. Reduction (and ultimately nitridation) was carried out in a 5% H_2/N_2 atmosphere yielding Fe, CaO, Cr_2O_3, and ZrO_2 as the reactive species, which formed various silicide and silicate phases during nitridation. No characterization of the metallic dispersion was conducted.

Following all nitridation runs, each piece of the nitridation apparatus that might possibly experience a mass change due to volatility (loss) or deposition (gain) was weighed on an analytical balance. This was done to ensure the accuracy of the acquired kinetic data, so that all weight changes measured by the TGA could be attributed to the proper source. Items that were post-weighed included the tungsten-basket support, the molybdenum crucible, and the Si–Si_3N_4 compact. No visible deposit ever appeared on the sapphire hangdown wire. Post-nitridation analysis of the microstructure was accomplished using optical

microscopy, and an SEM equipped with an energy-dispersive X-ray analyser. Quantitative phase composition was determined using nickel-filtered CuK_α X-ray diffraction [44].

3. Results and discussion

3.1. Influence of the furnace tube

Guthrie and Riley [26] were the first to recognize the possibility that oxide impurities derived from the furnace tube may be of significance during the nitridation of high-purity silicon wafers. In their analysis, four types of furnace tubes were used – two types of alumina, one made of sapphire, and another made from Coram (GEC Ltd). Based on XRD analysis for determination of the α/β phase ratio, they concluded that the ratio was influenced by the presence of trace impurities in the gaseous atmosphere. More specifically, the amount of α-phase produced was fairly constant over a range of conditions, but β-phase development varied quite significantly and was dependent on the type of alumina used. However, as also noted by the authors, the results were questionable. Sample sizes were notably small, ranging between 10 and 20 mg, and also possessed minimal surface area due to experimentation involving single crystals rather than finely divided powder. Hence, correspondingly small weight gains were observed. Ideally, one would prefer to maximize the available surface area for reaction in order to minimize spurious effects and facilitate post-analysis by XRD or other methods.

Of particular value, however, is the fact that attention was given to the impurities that could be derived from the furnace tube itself. This aspect appears to be lacking in much of the nitridation data reported in the literature. The furnace tube is inevitably some ceramic (due to the high temperatures involved) that may act as an infinite reservoir for key impurities such as oxygen and SiO among others. This is especially crucial because the nitridation mechanism appears to be influenced by the presence of oxygen, and may even be promoted at certain levels (see, for example, Section 3.2), while excess oxygen will retard nitridation due to SiO_2 formation which will act as a virtually impenetrable layer blocking the nitrogen gas from the underlying, unreacted silicon.

Typically, thermogravimetric analysis is used to study the nitridation kinetics. These high-temperature systems incorporate a ceramic hangdown tube of either mullite or high-purity alumina. Many mullite compositions possess about 15% glassy phase that yields relatively high vapour pressures for SiO and other impurities during nitridation. It is believed that impurities in the tube tend to segregate at the grain boundaries and develop substantial vapour pressures at these high reaction temperatures. Alumina, on the other hand, does not possess such a phase but still acts as a limitless source for oxygen and aluminium [26]. Our TGA experiments were conducted utilizing both mullite and alumina as the hangdown tubes (1in o.d. $\times$ 3/4in i.d. $\times$ 24in; 2.54 cm $\times$ 1.90 cm $\times$ 60.96 cm). Composition of the tubes is shown in Table I. A nitridation temperature of 1350 °C and a gas flow rate of 150 $cm^3\ min^{-1}$ of UHP 5% H_2/N_2 gas mixture was used for these nitridation runs. Reaction time was of the order of 20 h.

Fig. 2 illustrates the difference in the nitridation kinetics of unpromoted silicon powder resulting from the use of a furnace tube consisting of either mullite or high-purity alumina. Runs were conducted with and without a protective molybdenum lining inside the tube. The largest enhancement in the kinetics was observed in the runs with mullite alone. X-ray diffraction of samples did not show the presence of any deposited SiO_2 or $SiON_2$, so the weight gain was attributed solely to Si_3N_4 formation and not mere deposition of SiO_2.

Additional runs were conducted by first lining the mullite and alumina tubes with a thin foil of molybdenum, which served a two-fold purpose by blocking the flow of SiO_2, SiO and various metallic impurities into the reaction zone, and by acting as a getter for any residual oxygen flowing through the system. As expected, the rates and overall conversion were significantly lower than previously observed. An interesting observation is that the runs with either the lined-mullite or the lined-alumina exhibited similar nitridation behaviour, indicating the effectiveness of the molybdenum lining. Post-analysis of the white, crystalline, sand-like material that deposited on the molybdenum foil in the annular space between the

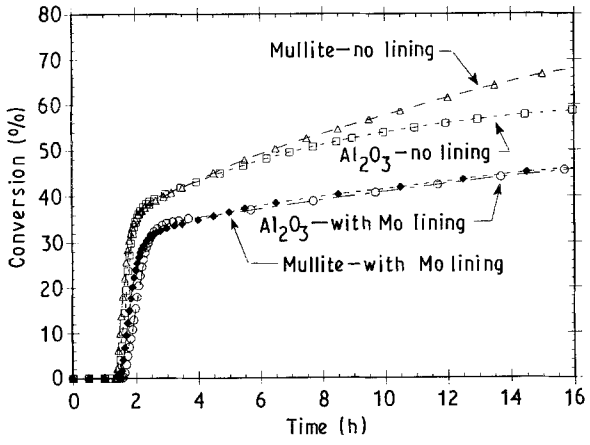

Figure 2 Influence on the nitridation kinetics resulting from the use of mullite or high-purity alumina furnace tubes (5–10 μm Si, 35 mg sample size, 1350 °C, 5% H_2/N_2, 150 $cm^3\ min^{-1}$).

TABLE I Chemical composition (wt %) of the hangdown tubes

Hangdown tube	Al_2O_3	SiO_2	MgO	Na_2O	CaO	Fe_2O_3	Cr_2O_3	TiO_2	B_2O_3	K_2O
Mullite MV30	60.0	38.0	0.2	0.2	0.1	0.5	–	0.5	–	0.7
Alumina 998	99.8	0.060	0.035	0.008	0.040	0.025	< 0.003	0.004	< 0.001	< 0.001

mullite tube and the foil itself was subjected to XRD analysis, Fig. 3. SiO_2 (cristobalite; JCPDS 11-695) was determined to be the main constituent. Other species present at much lower concentrations included SiO_2 (tridymite; JCPDS 14-260), Si, MoO_3 (molybdite; JCPDS 5-508), and Al_2O_3 (JCPDS 13-373 and 23-1009). No molybdenum, Si_2ON_2, α-Si_3N_4, or β-Si_3N_4 was found within the detection limits of the XRD. A similar deposit, but at a much lower concentration, was found on the foil surface exposed to the flowing atmosphere immediately below the hot zone of the furnace; its presence was due to a vertical seam in the molybdenum foil that allowed a very minor amount of the mullite gases to pass through the reaction area.

When an unlined high-purity alumina tube was used, nitridation kinetics were enhanced above that observed with the molybdenum-lined mullite or molybdenum-lined alumina, but to a lesser extent than for the unlined mullite. This indicated a similar enhancement of the process by SiO nitridation resulting from the alumina tube acting as a limitless source of oxygen gas when heated to reaction temperatures.

In separate experiments [45] to determine the volatility of SiO under various experimental conditions, 100 mg samples of solid silicon monoxide were charged to a tantalum crucible (7 mm diameter) monitored by a TGA system. Heating was at a rate of 1200 °C h^{-1} under flowing helium with $< 5 \times 10^{-7}$ atm (< 0.5 p.p.m.) oxygen content. Condensible crystalline phases detected by XRD indicated the formation of silicon and SiO_2 in the cristobalite form, as was encountered in the experiments discussed above.

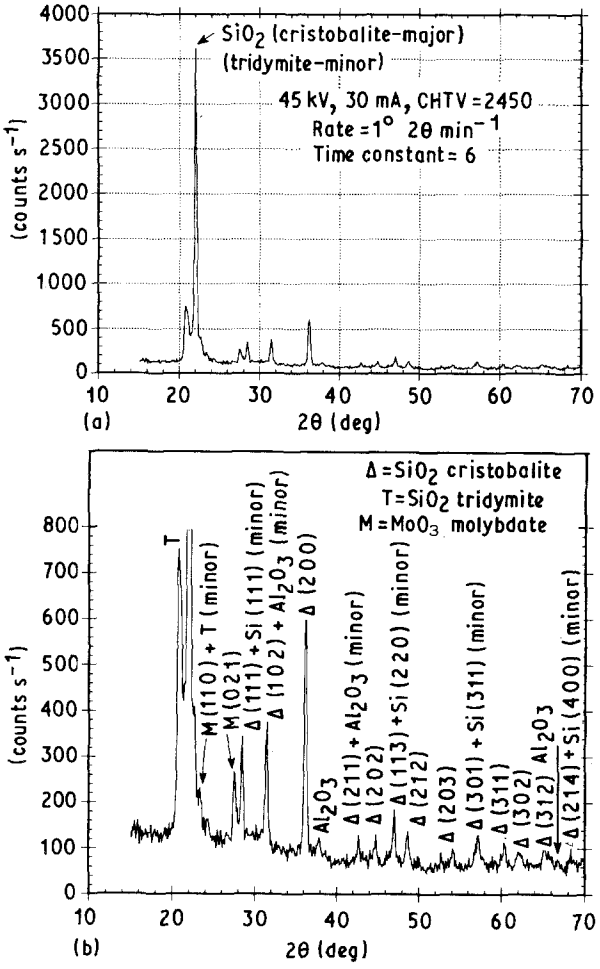

Figure 3 XRD pattern (CuK_α) of the deposit accumulating in the annular space between the mullite tube and the molybdenum foil: (a) full-scale XRD profile showing the major SiO_2 peak; (b) magnification of same profile showing detail of all smaller peaks.

3.2. Equilibrium analysis for the feasibility of SiO nitridation

Table II summarizes the pertinent reactions for the nitridation of SiO(g). The data reflects the calculated concentrations of various species at 1350 °C under high-purity conditions, and indicates the relative importance of a given reaction under three model situations: (a) 0% H_2 added to the nitriding gas incorporating a molybdenum-lined furnace tube, (b) 5% H_2 added with a molybdenum-lined furnace tube, and (c) 5% H_2 added using an unlined furnace tube.

While our experimental results clearly indicate a pronounced contribution to the observed nitridation kinetics resulting from SiO nitridation by Reaction 1 of Table II, different opinions exist in the literature regarding its feasibility due to the large and positive ΔG, which suggests otherwise. Based on their analysis of experimental data, Dervisbegovic and Riley [35] concluded that SiO was, in fact, not involved in the silicon nitridation process; Jennings [12] indicated that the process is doubtful in the absence of added hydrogen; Moulson [11] suggested a limited contribution under specific conditions; while Riley [46] proposed it may be involved in a silicon monoxide regeneration cycle (via Reactions 1 and 2); and Lindley *et al.* [32] assumed that, even in the absence of hydrogen (which could generate SiO through a reaction with surface silica; Reaction 7 in Table II), SiO is a major source of the α-phase and that silicon surfaces and silicon vapour can adequately lower p_{O_2} through reaction to form SiO_2(s), thus shifting Reaction 1 to the right. Hence the obvious question arises as to whether or not SiO is a significant factor in the formation of Si_3N_4 under typical nitridation conditions (1350 °C, 1 atm N_2).

In the following analysis, we attempt to demonstrate how the thermodynamics are markedly altered in favour of SiO nitridation in a "high-purity" system (10^{-6}–10^{-8} atm O_2 and H_2O) by the presence of 5% H_2 and an unlined mullite tube, by focusing on the reactions listed in Table II. We initially investigate equilibrium conditions for nitridation without added hydrogen or contributions from the mullite tube, and then subsequently follow with 5% H_2 addition, and then the mullite tube. The main caveat to the analysis is the assumption of local equilibrium within the inner domain of the compact. While this assumption may seem somewhat tenuous, it is probably a reasonable approximation of the actual process, at least for a preliminary analysis. In spite of this recognized difficulty, previous workers [11, 12, 32, 35, 46] have also made similar assumptions.

TABLE II Equilibrium reactions involved in the nitridation of SiO(g) under typical "high-purity" conditions

	Equilibrium Reaction	$\Delta G_{(1350\,^{\circ}C)}$ (kJ mol^{-1})	Key features of pertinent reactions under "high-purity" conditions (1×10^{-6} atm O_2 and H_2O; 1350° C) (Partial pressures in atm)		
			0% H_2 with lined tube	5% H_2 with lined tube	5% H_2 with unlined tube[a]
(1)	$3\,SiO(g)+2\,N_2(g) \rightleftharpoons Si_3N_4(s)+\frac{3}{2}O_2(g)$	+502	$p_{O_2}\leqslant 3.1\times10^{-16}$ (required in rxn zone)	H_2 removes O_2 thereby enhancing Reaction 6 $\Rightarrow p_{O_2}=2.8\times10^{-19}$	$p_{O_2}\leqslant 1.7\times10^{-15}$ (required in reaction zone)
(2)	$2\,Si(s)+O_2(g) \rightleftharpoons 2\,SiO(g)$ (active oxidation)	−477	→RHS $p_{SiO}=2p_{O_2}=2\times10^{-6}$	→RHS no significant contribution due to p_{O_2} decrease by H_2	(Same)[b]
(3)	$Si(s)+O_2(g) \rightleftharpoons SiO_2(s)$ (passive oxidation)	−620	→RHS Cycle with Reactions 4 and 7 followed by Reaction 1	→RHS still contributes to SiO_2 formation	(Same)[b]
(4)	$SiO_2(s)+Si(s) \rightleftharpoons 2\,SiO(g)$	+147	$p_{SiO}=4.3\times10^{-3}$ (theoretical limit determined by temperature)	(Same)	Transient $p_{SiO}=10^{-2}$ in excess of equilibrium; disproportionation occurs
(5)	$Si(s)+H_2O(g) \rightleftharpoons SiO(g)+H_2(g)$	−84	→RHS $p_{H_2}=p_{SiO}$ limited by $p_{H_2O}=10^{-6}$	→RHS $p_{H_2}=p_{SiO}=3\times10^{-6}$ (still limited by p_{H_2O})	SiO will disproportionate if $p_{H_2O}<9.9\times10^{-7}$
(6)	$2\,H_2(g)+O_2(g) \rightleftharpoons 2\,H_2O(g)$	−314	→RHS (determines reaction zone p_{H_2O}) $\leqslant 2.0\times10^{-9}$ required for Reaction 1	→RHS (determines reaction zone p_{H_2O}) $\leqslant 1.0\times10^{-4}$ required for Reaction 1	→RHS (determines reaction zone p_{H_2O}) $\leqslant 2.3\times10^{-4}$ required for Reaction 1
(7)	$SiO_2+H_2(g) \rightleftharpoons H_2O(g)+SiO(g)$	+230	$p_{SiO}=4.9\times10^{-3}$ near silicon surface (significant SiO source)	$p_{SiO}=4.7\times10^{-3}$ near silicon surface (significant SiO source)	SiO will disproportionate if $p_{H_2O}>2.0\times10^{-7}$

[a] Assuming unlined mullite yields $p_{SiO}=0.01$ atm in bulk phase.
[b] No change in reaction behaviour relative to previous nitriding conditions presented on immediate left.

3.2.1. *SiO nitridation with 0% H_2 added using a lined furnace tube*

Assuming ideal gas behaviour, the extent of a given reaction is defined at equilibrium by

$$-\frac{\Delta G}{RT} = \ln(K) \tag{8a}$$

$$K = \prod_{i=1}^{\text{species}} (p_i^{\nu_i}) \tag{8b}$$

where p_i are the partial pressures of the gaseous species (atm), and ν_i are the corresponding stoichiometric coefficients (positive for products and negative for reactants). Calculations show that Reactions 4 and 7 are the dominant ones controlling the concentration of SiO(g) at any given time, yielding partial pressures of 4.3×10^{-3} and 4.9×10^{-3} atm, respectively. Even though Reaction 2 has a large and negative ΔG, which indicates that products are favoured, the concentration of SiO(g) following this reaction is limited by the residual O_2 (10^{-6} atm) in the nitriding gas, and therefore, this reaction contributes minimally to SiO(g) formation. When attention is given to ensuring high-purity nitridation conditions (by the use of UHP gases and various getters) the bulk O_2 and H_2O concentrations would be expected to vary between 10^{-6} atm (1 p.p.m.) down to 10^{-8} atm (10 p.p.b.), and hence, SiO(g) via Reaction 2 would be limited to the same partial pressures. Likewise, the formation of SiO(g) via Reaction 5 is limited by the residual H_2O. In short, Reaction 4 indicates there is a theoretical maximum value of SiO(g), due to disproportionation, of 4.3×10^{-3} atm at 1350 °C. This argument indicates that p_{SiO} is not determined by residual O_2 or H_2O, as has been assumed in previous analyses [11, 12], but rather it is dominated by the devitrification of surface $SiO_2(s)$ to form SiO(g) via Reaction 7, and by the nitridation temperature following Reaction 4, Fig. 4.

The likely route for SiO nitridation would consist of the following sequence. Initially, exposed silicon would react with the residual oxygen through passive oxidation to form a layer of $SiO_2(s)$ ($\approx$3 nm) on the surface of the silicon particles via Reaction 3. Owing to a very large and negative ΔG (-620 kJ mol^{-1}), it is unlikely that there would be exposed silicon for an extended period of time during the course of nitridation, i.e. the reaction strongly favours product formation. The $SiO_2(s)$ layer would then react with Si(s) via Reaction 4 and with $H_2(g)$ via Reaction 7 to form SiO(g), and hence, determine p_{SiO} ($>10^{-3}$ atm). Both

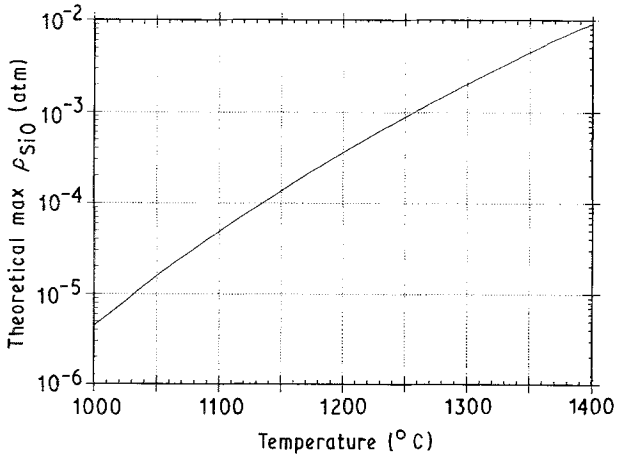

Figure 4 Theoretical maximum concentration of SiO(g) as a function of nitridation temperature, due to the disproportionation reaction to form Si(s) and SiO_2(s) (Reaction 4, Table II).

Reactions 4 and 7 represent heterogeneous formation of SiO(g) occurring at the particle surfaces, and thus reflect p_{SiO} in the adjacent vapour phase. SiO(g) would subsequently react to form Si_3N_4 following Reaction 1. The H_2(g) required for Reaction 7 is generated by Reaction 5 which yields a p_{H_2} equivalent to the residual p_{H_2O} of 10^{-6} atm due to the large and negative ΔG. The p_{H_2O} used for the calculation of p_{SiO} via Reaction 7 involves its equilibrium concentration also determined by Reaction 5, because this reaction represents the behaviour near the silicon surface.

However, in order for Reaction 1 to contribute significantly to the observed nitridation rates, certain thermodynamic criteria need to be met. With $p_{SiO} = 4.3 \times 10^{-3}$ atm (theoretical limit; Reaction 4) and $p_{N_2} = 1$ atm, Reaction 1 suggests that p_{O_2} would correspondingly be required to be $\leqslant 3.1 \times 10^{-16}$ atm in the zone of formation in order for the reaction to proceed. This zone refers to a hypothetical region located between adjacent silicon particles, i.e. somewhere in the concentration gradient between the bulk phase and the surface of the particles, where conditions for Reaction 1 are satisfied. As was noted by Moulson [11], the oxygen flux out of the reaction zone will control the rate of SiO nitridation. Reaction 3 (passive oxidation) indicates a p_{O_2} near the surface of oxidation of the order of 1.1×10^{-20} atm, while Reaction 2 (active oxidation) indicates a p_{O_2} of 8.2×10^{-21} atm, both yielding partial pressures much lower than that required in the reaction zone. Hence, exposed silicon provides an adequate oxygen sink, yielding a positive oxygen gradient away from the reaction zone, and therefore SiO nitridation can make a significant contribution to the observed rates.

Analogous to Reactions 2 and 3, Reaction 5 strongly favours product formation. As was noted previously, this suggests p_{H_2} would be limited by the residual H_2O concentration (10^{-6}–10^{-8} atm). Hence with p_{H_2} between 10^{-6} and 10^{-8} atm, Reaction 6 indicates that

$$\frac{p^2_{H_2O}}{p_{O_2}} = 1.3 \times 10^{-2} \text{ to } 1.3 \times 10^{-6} \quad (9)$$

This determines the required p_{H_2O} in the reaction zone. With the condition of $p_{O_2} \leqslant 3.1 \times 10^{-16}$ atm, p_{H_2O} would therefore need to be $\leqslant 2.0 \times 10^{-9}$ to $\leqslant 2.0 \times 10^{-11}$ atm to sustain Reaction 1. If p_{H_2O} were greater than this, Reaction 6 would shift to the left thereby increasing p_{O_2} above the maximum limit. These low partial pressures of H_2O may seem unlikely to occur within the compact, however, they can be readily achieved upon noting Reaction 5, which suggests that for $p_{SiO} = 4.3 \times 10^{-3}$ atm and $p_{H_2} = 10^{-6}$–10^{-8} atm, p_{H_2O} would be correspondingly lowered to 8.1×10^{-12} to 8.1×10^{-14} atm, values meeting the necessary requirement. As in the case of silicon oxidation (Reactions 2 and 3) in producing the necessary oxygen gradient for Reaction 1 to proceed, Si(s) reacting with H_2O(g) (Reaction 5) provides a favourable gradient to achieve the required p_{H_2O} in the reaction zone. Fig. 5a summarizes the equilibrium requirements within the inner domain of the silicon compact for nitridation under "high-purity" conditions.

3.2.2. SiO nitridation with 5% H_2 added using a lined furnace tube

By addition of 5% H_2 (5×10^{-2} atm) to the nitriding atmosphere, the thermodynamics are altered to render SiO nitridation even more favourable. Reaction 6 indicates that the ratio $p^2_{H_2O}/p_{O_2}$ increases to 3.2×10^7 atm. For $p_{H_2O} = 3 \times 10^{-6}$ atm (residual 10^{-6} atm plus 2×10^{-6} atm due to Reaction 6), this suggests a lowering of p_{O_2} in the bulk phase to 2.8×10^{-19} atm. Therefore, the oxygen partial pressure requirement in the Si_3N_4 formation zone of $\leqslant 3.1 \times 10^{-16}$ atm can more readily be achieved through the shifting of Reaction 6 to the right. Furthermore, there is an easing of the restriction on p_{H_2O} in the reaction zone from $\leqslant 2.0 \times 10^{-9}$ atm to $\leqslant 1.0 \times 10^{-4}$ atm. Obviously this requirement can readily be met as it is a partial pressure greater than the residual impurity level (10^{-6} atm) of the nitriding gas, so that p_{H_2O} is no longer a factor in determining SiO reaction equilibrium in the formation zone.

In spite of the added H_2(g), Reaction 7 does not contribute to the production of SiO(g) any more significantly than was observed without the additional H_2(g). This is due to the increased p_{H_2O} near the particles surfaces resulting from the shifting of Reaction 5 to the left. p_{H_2O} near the silicon surfaces will be of the order of 4.2×10^{-7} atm, up from the 8.1×10^{-12} atm observed when no hydrogen was added. The calculated p_{SiO} generated by Reaction 7 is 4.7×10^{-3} atm, essentially identical to the 0% H_2 case, and therefore this reaction is still a significant source of SiO(g).

Active oxidation (Reaction 2) no longer contributes to the production of SiO(g) to any appreciable extent due to the lowering of p_{O_2} from 10^{-6} atm to 2.8×10^{-19} atm by Reaction 6. Previously, active oxidation was able to form SiO(g) at a level identical to the residual p_{O_2} of 10^{-6} atm. On the other hand, passive oxidation to form SiO_2(s) (Reaction 3) is still a source of this necessary reactant which supplies SiO_2(s) to

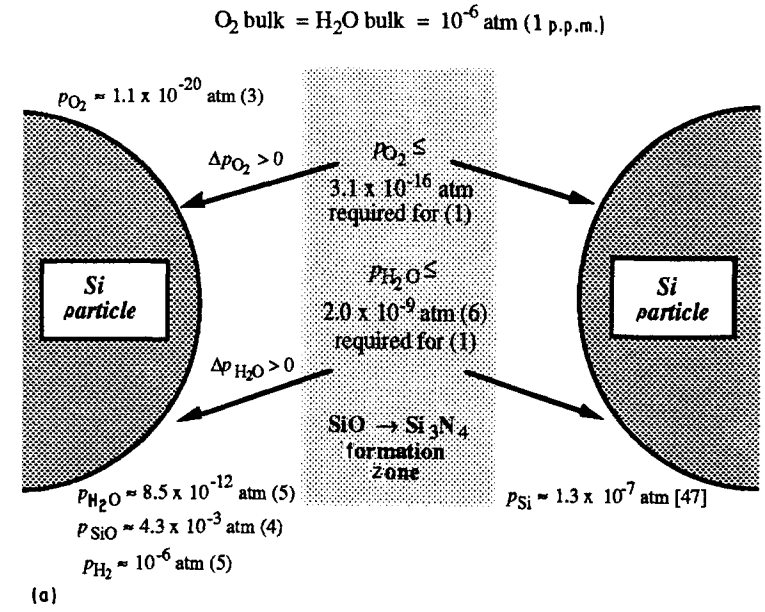

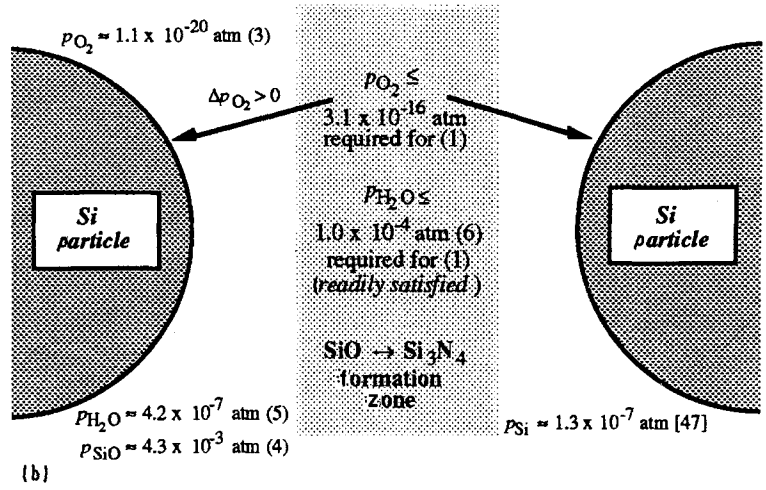

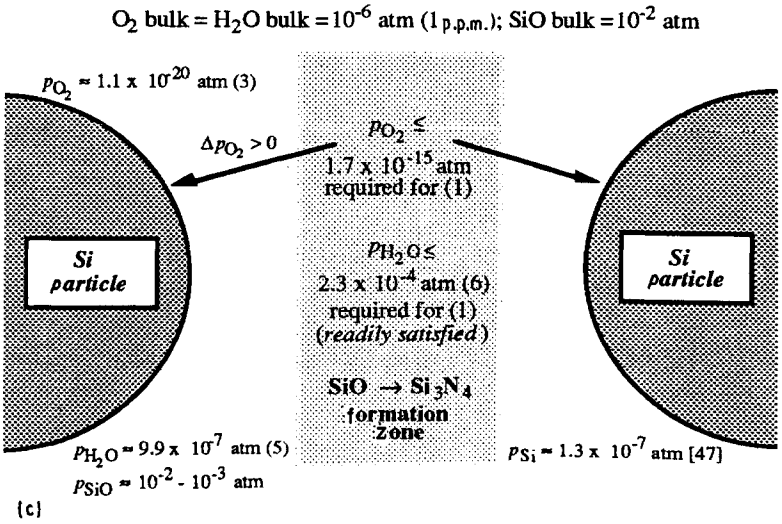

Figure 5 Theoretical concentrations required for the nitridation of SiO within the inner domains of a silicon compact at 1350 °C. Conditions presented at 1 atm total pressure for (a) "typical" high-purity atmosphere, (b) 5% H_2/95% N_2, and (c) 5% H_2/95% N_2 with unlined furnace tube. Numbers in parentheses indicate relevant reactions listed in Table II. Partial pressures are near the silicon surface. (Adapted from Moulson [11].)

Reactions 4 and 7. As noted in Section 3.2.1, the equilibrium p_{O_2} for this reaction is of the order of 1.1×10^{-20} atm, a value lower than that established by Reaction 6. Fig. 5b summarizes the conditions for nitridation with 5% H_2 in the presence of a molybdenum-lined furnace tube.

3.2.3. SiO nitridation with 5% H_2 added using an unlined furnace tube

When nitridation is carried out in presence of an unlined mullite tube, an external source of SiO is available. Considering the decomposition reaction

$$\begin{aligned} SiO_2(s) &\rightleftharpoons SiO(g) + \tfrac{1}{2}O_2(g) \\ \Delta G_{1350°C} &= 385\ kJ\ mol^{-1} \end{aligned} \quad (10)$$

the equilibrium p_{SiO} in the presence of 5% H_2 is approximately 7.7×10^{-4} atm. This quantity is slightly less than the theoretical limit of 4.3×10^{-3} atm (Reaction 4) and represents the behaviour of pure, single-crystalline SiO_2(s). Clearly this is not the case for an unlined mullite tube that notably consists of 15% glassy phase. It is reasonable to assume that the quantity of SiO(g) generated from the tube would likely be in excess of this theoretical value, especially considering the large deposits that were observed and subsequently analysed by XRD. Hence, transient SiO concentrations on the order of 10^{-2} atm may be produced, followed by disproportionation (Reaction 4) to produce SiO_2 and silicon. So the ultimate contribution of the mullite tube would be manifest through SiO(g) (via Reaction 1), SiO_2 (via Reactions 4 and 7 followed by Reaction 1), and silicon which could react in the usual manner. Assuming $p_{SiO} = 10^{-2}$ atm, Reaction 1 suggests that the requirement for p_{O_2} in the reaction zone to be eased from $\leqslant 3.1 \times 10^{-16}$ atm to $\leqslant 1.7 \times 10^{-15}$ atm, and similarly for p_{H_2O}, from $\leqslant 2.0 \times 10^{-9}$ atm (0% H_2 and molybdenum-lined tube) to $\leqslant 2.3 \times 10^{-4}$ atm (with 5% H_2 and unlined mullite), conditions which can be readily attained based on the previous thermodynamic considerations, Fig. 5c.

With SiO(g) partial pressures in excess of the theoretical limit (4.3×10^{-3} atm), disproportionation will occur by Reactions 4, 5 and 7. Reaction 5 indicates that SiO(g) decomposition will occur if $p_{H_2O} < 9.9 \times 10^{-7}$ atm, while Reaction 7 indicates similar behaviour if $p_{H_2O} > 2.0 \times 10^{-7}$ atm. Fig. 5c summarizes the conditions observed when nitriding in 5% H_2 using an unlined furnace tube.

3.2.4. Concluding remarks on SiO nitridation

In summary, it appears that SiO nitridation (Reaction 1) is not only feasible, but that it is a significant contributor to the observed nitridation rates under "high-purity" conditions. Even in the absence of added hydrogen, the process is thermodynamically possible in spite of the large and positive ΔG, i.e. gradients are favourable for the removal of oxygen from the reaction zone, which likely determines the rate of Reaction 1. Additionally, oxygen appears to be favourable to the nitridation process at levels encountered under typical high-purity conditions (10^{-6}–10^{-8} atm). Its contribution diminishes as concentrations become excessive, however, by causing prohibitively large SiO_2(s) production, thereby minimizing exposure of the silicon surface and shifting conditions away from equilibrium.

The reaction between SiO_2(s) and Si(s) (Reaction 4), along with the reaction between SiO_2(s) and H_2(g) (Reaction 7), are the main sources of SiO(g) when nitriding in both the presence or absence of added H_2(g). Active oxidation of Si(s) (Reaction 3) is a minor contributor to SiO(g) formation. The theoretical limit of SiO(g) is determined by the reaction temperature following Reaction 4, Fig. 4. Any excess SiO(g) will likely undergo decomposition to form either SiO_2(s) or Si(s). However, transient concentrations of greater value can occur when nitriding with an unlined furnace tube.

The use of an unlined mullite or alumina furnace tube at typical nitridation temperatures will act as an infinite reservoir for volatile SiO_2 and SiO, which have a marked influence on the nitridation kinetics by uninhibited vaporization of these species, followed by vapour-phase reaction of SiO to form Si_3N_4 (predominantly α-phase).

This issue of contamination derived from the furnace tube is a salient and pertinent aspect rarely given appropriate attention in experiments reported in the literature. Kinetic data that are to be subjected to quantitative analysis must acknowledge this aspect, and suitably address this concern prior to its acquisition by the use of some type of material (such as molybdenum, titanium or zirconium) that will both getter oxygen and, more importantly, physically block the transport of other volatile species (such as SiO, SiO_2, and various metallic impurities) originating from the ceramic furnace tube at nitridation temperatures.

3.3. Silicon packing effects: free powder versus compact behaviour

The packing of particles in the range of 0.1–100 μm is of particular interest in powder metallurgy where a compact is desired as the starting point in the production of a product (e.g. [48–55]). As expected, the microstructure of the green compact plays a crucial role in the nitridation of silicon, and also in the mechanical integrity of the resulting product. Final pore size, shape, and distribution, which are major factors influencing strength [56–58], are strongly influenced by the initial structure of the green compact [59].

Full conversion becomes increasingly difficult as the green density of the compact increases, and thus one would expect the existence of an optimum or maximum preform density which can be successfully nitrided without unreacted silicon remaining. Ideally there would be just the right amount *and* type of porosity (dependent on particle size, shape, compaction pressure and technique) to ensure complete pore closure at the same instant full conversion of the individual grains is achieved. A first step in this realization would

be careful classification and characterization of the starting silicon powder to ensure reasonably spherical particles of a narrow size distribution. In this light, the nitridation kinetics of strictly classified, high-purity silicon powder have recently been investigated in detail, to ascertain particle size and compact effects on the intrinsic behaviour [15].

Indeed, much of the variability in the kinetics, especially with regards to extent of conversion, that has been reported in the literature can be attributed to subtle deviations in the packing of the green compacts, more so than any other single aspect affecting the process. Particle shape and size distribution also significantly influence the kinetics. While these two latter factors may not govern the process in as strong a manner as temperature, nitriding atmosphere, and pressure, they do play a crucial role in the structural formation of the final product owing to the unique nature of RBSN compared to most other ceramics.

Preliminary experiments have demonstrated the telling influence on the nitridation kinetics resulting from variations in the particle size and green density of the silicon compact. Fig. 6 shows the nitridation curves for unpromoted silicon of two sizes: -43 μm (4.16 μm average Fisher size) and -250 μm diameter powder. Packing density was determined by volume and mass measurements, yielding green densities, relative to crystalline silicon (2.33 g cm^{-3}), of 43.5% and 45.5% for the -250 and -43 μm free powder, respectively, while the compacted (110000 p.s.i.) silicon had green densities of 61.2% and 71.4%, respectively.

As the particle radius increases, the reactive area (i.e. the external surface of the silicon particles) per unit mass, decreases. Clearly, this inhibits the overall rate and conversion by reducing the available contact area between the nitrogen and silicon, and by reducing the surface area available for silicon vaporization. Diffusion of nitrogen through the silicon may occur, but at many orders of magnitude less than gas-phase diffusion, and hence its contribution to the observed kinetics is negligible. However, this route of nitridation may be the only feasible one available during the final stages of nitridation when other dominant pathways are no longer viable due to pore closure, densification, and grain coarsening.

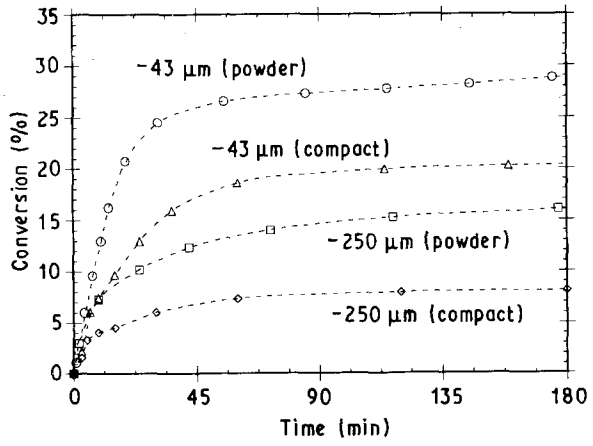

Figure 6 Nitridation kinetics for silicon powder and silicon compacts of varying size, clearly demonstrating the effect of reactive surface area and pore availability for nitrogen diffusion on the overall rate and conversion (unlined mullite tube, 1350 °C, 5% H_2/N_2, 150 cm^3 min^{-1}).

Nitriding compacted silicon results in a similar effect – but in this case, reduction of pore size *between* the particles is the reason. A distinction must be made regarding the macropore structure (typically greater than ≈ 1 μm), determined by the efficiency of the packing, and the micropore structure (typically 10 nm to < 0.1 μm), determined by the relative integrity of the Si_3N_4 product layer surrounding each particle, and how the characteristic 21.7% volume expansion is incorporated into the macropore structure. The calculated mean free path of nitrogen at 1350 °C is approximately 4.0 μm, while that of hydrogen is approximately 8.7 μm; this is of the order of the particle size and macropore porosity. Hence, Knudsen diffusion ($D_{eff} \approx 10^{-2}$–10^{-5} cm^2 s^{-1}) likely plays a significant role in the transport of both hydrogen and nitrogen in the nitridation of *compacted* silicon.

This aspect is crucial, noting the dramatic role hydrogen plays in the nitridation process: (1) devitrification of inherent SiO_2 layer (≈ 3 nm typical) [34, 35, 42], (2) contribution to favourable thermodynamics for SiO nitridation (as was described in Section 3.2.2), and (3) strength enhancement noted by marked improvement in mechanical properties [28, 30, 32]. Nevertheless, pore-size reduction and its concomitant effect on lowering diffusion of reacting species is not limited to compacts alone.

Mass transport in the nitridation of free powder also involves Knudsen diffusion in the *later* stages of reaction as the outer surface develops a dense layer of α-Si_3N_4, followed by a general trend of pore filling and density increase throughout inner domains of the macropore structure. This is applicable in all nitriding situations where grains of silicon are close enough together such that adjacent particles reaction bond, thereby reducing the macroporosity. Hence, the overall effective diffusivity through the macropore structure appears to involve a transition from pure binary diffusion (at the onset and early stages of nitridation), to that of Knudsen diffusion (as the product layer develops). This behaviour eventually culminates in diffusion characterized by transport of gas in relatively non-porous Si–Si_3N_4, under conditions referred to as *configurational* diffusion ($D_{eff} < 10^{-5}$ cm^2 s^{-1}) [60]. As the relative contribution of binary diffusion succumbs to Knudsen diffusion, the reaction rate decreases dramatically, and the characteristic kneeing in the conversion versus time behaviour is observed. Overall, through porosity tends to become restricted, resulting in a transition from kinetic limitation (initially) to that of diffusional limitation.

This idea is further elucidated in the scanning electron micrographs of Fig. 7, showing the top view of a nitridation sequence of *free* silicon powder resting in a crucible. In the very initial stages, whisker growth from the surface on each of the individual grains emanates into the space between the particles, Fig. 7a. At this stage, nitrogen diffuses freely throughout the

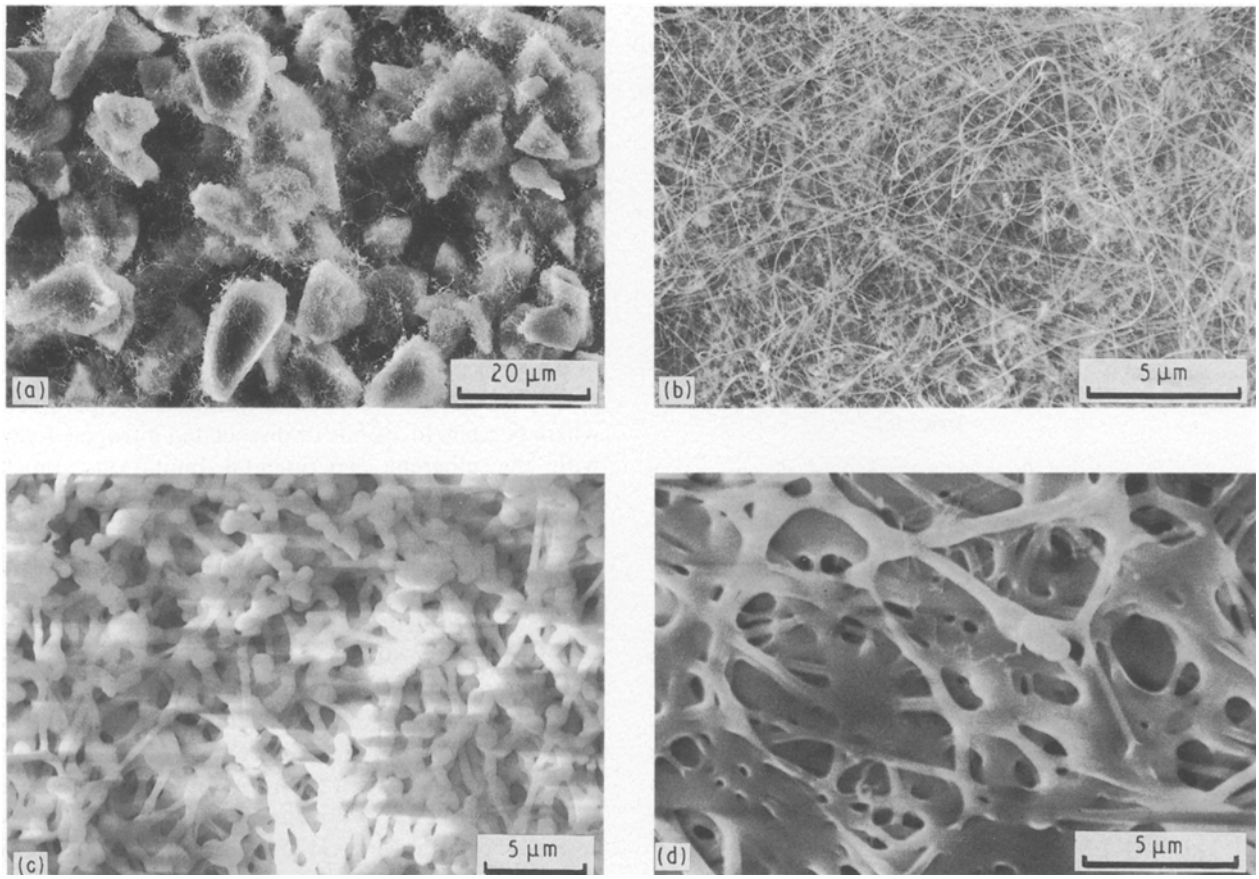

Figure 7 Scanning electron micrographs of the top surface of uncompacted 5–10 μm silicon powder during nitridation at 1350 °C in 5% H_2/N_2 at 150 cm^3 min^{-1}. (a) 5 min after reaction initiation (×1160), (b) 1 h (×5500), (c) 12 h (×3500), (d) 50 h (×5500).

macroporosity. With further reaction, the whisker matte becomes extensive, covering the entire outer surface of the free powder, Fig. 7b. A cross-section at this stage in the reaction would reveal a watermelon-like shell that encompasses the sample. Nitrogen diffusion is inhibited, and the characteristic kneeing in the kinetic data is observed. As time progresses, sintering and densification of the outer shell occurs, further restricting the diffusion of reacting species into the sample, Fig. 7c and d.

3.4. Pre-sintering effects

In developing a silicon compact with sufficient integrity such that machining can be done prior to nitridation, pre-sintering in an inert atmosphere is typically carried out at elevated temperatures ($\sim$ 1200 °C [61]). This practice was adapted to take advantage of one of the remarkable features of the reaction-bonding process, that being the retention of the overall external dimensions of the green compact to within about 0.1% during the transformation from silicon to Si_3N_4. This behaviour suggests that surface diffusion and/or vaporization/condensation mechanisms are operative. Recent data of Coblenz [62] and Robertson [63] indicate that surface diffusion is the dominant mass-transport path for the sintering of pure silicon particles. While full conversion of the compact to the nitride ceramic does not necessarily imply the absence of porosity, and indeed rarely does, it does occur without significant shrinkage of the compact. Post-densification, via hot pressing or pressure sintering at temperatures between 1700 and 1800 °C, is required to achieve densities approaching theoretical. As expected, shrinkage will occur during this process to eliminate voids, the extent being directly related to the maximum density achieved following reaction bonding.

Pre-sintering tends to have adverse effects on the microstructure of the green compact. In addition to causing void formation [61], the sintering process inherently predicates changes in the macroscopic porosity. Fig. 8 further supports the ideas presented in Fig. 6 by demonstrating the effect of silicon-particle sintering prior to nitridation. Runs were conducted by varying the exposure time of the < 10 μm silicon between 0 and 6 h at 1350 °C in a 5% H_2/95% Ar mixture. Following pre-sintering, the samples were then nitrided in the standard mixture of 5% H_2/95% N_2 at 1350 °C.

Pore size and distribution are altered via neck formation between adjacent particles, resulting in a reduction in the available silicon surface area, and further impeding the diffusion of reactant species into the inner domains of the compact. As was noted in Section 3.3, a reduction in silicon surface area corresponds both to a reduction in silicon vaporization (a key factor influencing intrinsic nitridation rates) and sites available for Si_3N_4 nucleation. Longer sintering times correspond to a greater reduction in overall

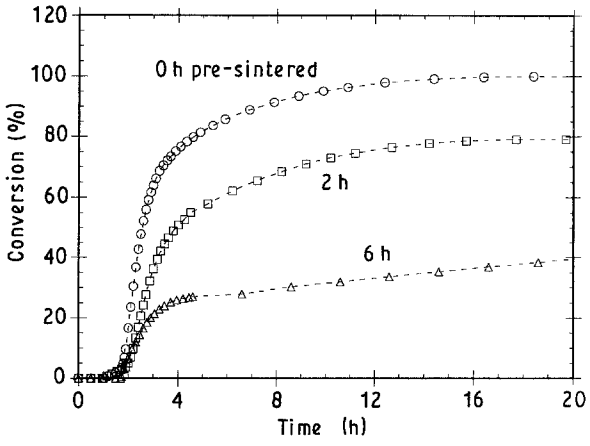

Figure 8 Pre-sintering effects on the rate and overall conversion of silicon powder, (5–10 μm Si, 20 mg sample size, 1350 °C, 5% H_2/N_2, 150 cm^3 min^{-1}).

conversion and rate of nitridation. To our knowledge, this effect has not been explicitly acknowledged in previous literature, although its practice appears to be quite acceptable and is commonly used in industry, and is also used sometimes in research during the devitrification of the inherent SiO_2 layer ($\approx$3 nm typically) in a hydrogen or hydrogen-containing atmosphere prior to the actual nitridation process. This latter use is inappropriate if the intention is to obtain kinetics for a given particle-size distribution, where its size and surface area are typically determined previously at room temperature.

3.5. Influence of liquid phase and atomic nitrogen formation

The formation of a liquid phase by metal silicide or silicate formation from metal or metal-oxide additions greatly enhances the rate and extent of both nitridation and densification. In the case of iron, there is little disagreement that its presence markedly influences the observed nitridation behaviour during the nitridation of silicon compacts [19, 25]. The enhancement has been attributed to three main factors: (1) devitrification of the inherent SiO_2 layer [25] by possibly providing nucleation sites for the devitrification process [64]; (2) through the formation of low-eutectic silicide phases [11, 19] which provide alternate, rapid nitrogen diffusion paths (stimulating production of β-Si_3N_4 [19]) and act as a source of volatile silicon (a precursor for one of the accepted mechanisms of α-Si_3N_4 synthesis [65]); and (3) by promoting the formation of atomic nitrogen as in catalysis of ammonia synthesis. This latter aspect of the ability of the cation element to encourage dissociative chemisorption of nitrogen has been the subject of debate, because, as was noted by Jennings [66], no supporting experimental evidence has been demonstrated in its favour.

In this light, a systematic approach seems most plausible, with the intention of minimizing the effects of other reaction parameters while focusing on one, in this case, the formation of active nitrogen. Ideally, an experiment would be designed such that nitridation conditions were identical for all reaction parameters, such as temperature, flow rates, particle size, etc., except for the relative ability of the added cation to either dissociate nitrogen or form liquid phase. Obviously this ideal situation is unlikely to be achieved fully, but nevertheless, it is approachable to a reasonable extent. One can envision a series of experiments in which attention is solely directed towards the issue of liquid phase and dissociated nitrogen formation, all other factors remaining essentially constant. Metal additives can then be categorized into one of four areas: liquid/N, no liquid/N, liquid/N_2, and no liquid/N_2 at the selected nitridation temperature, where N refers to atomic or dissociated nitrogen. Even with the inherent experimental limitations, much could be gained by studying the nitridation behaviour under the four scenarios stated above, through careful selection of the additives to approximate ideal conditions.

The active-nitrogen question can be resolved by comparing the results of a series of experiments using silicon impregnated with a metal known to dissociate N_2(g), e.g. iron, and one not likely to have a dissociative effect on N_2(g), e.g. zirconium. If dissociated nitrogen is a factor, then the nitridation rates observed at 1185 °C, which is below the Fe/Si (1200 °C [67]; no liquid/N) and the Zr/Si (1355 °C [68]; no liquid/N_2) eutectics, are expected to be greater for iron than for zirconium. If the catalytic activity of iron carries over to the silicide melt, then the nitriding rate (at say 1370 °C) of the iron silicide melt (liquid/N) should also be superior to that of the zirconium silicate melt (liquid/N_2).

Fig. 9 elucidates the effect of dissociated nitrogen on the nitridation process. Samples were impregnated at 0.3 at % (0.59 wt %) Fe and 0.3 at % Zr (i.e. 1.30 wt % ZrO_2) loadings, and nitrided in the manner described above. The results indicate that iron does indeed dissociate nitrogen, with the concomitant enhancement to the nitridation process, its rate being greater than the zirconium-impregnated samples at both 1185 °C (Fig. 9a) and 1370 °C (Fig. 9b). At 1185 °C, where no liquid was present in either case, it appears that zirconium was able to dissociate nitrogen due to the high reaction temperature (albeit much less effectively than iron), or was perhaps involved in the enhanced devitrification of the SiO_2 layer. This was discernible by comparison of the 0 at % versus 0.3 at % Zr. If nitridation conditions were ideal, then both runs would have yielded identical behaviour, because neither was expected to have liquid phase or atomic nitrogen. Regardless of this deviation from ideality, the nitridation enhancement observed for the iron and zirconium runs can likely be attributed to the effects of dissociated nitrogen and the removal of SiO_2.

The runs at 1370 °C, Fig. 9b, clearly demonstrate that the presence of *both* a liquid phase and dissociated nitrogen, yields nitridation rates over and above that observed by just one of the enhancement factors alone. This was observed by a comparison of the iron-promoted sample with the zirconium and metal-free runs. The iron-promoted sample achieved

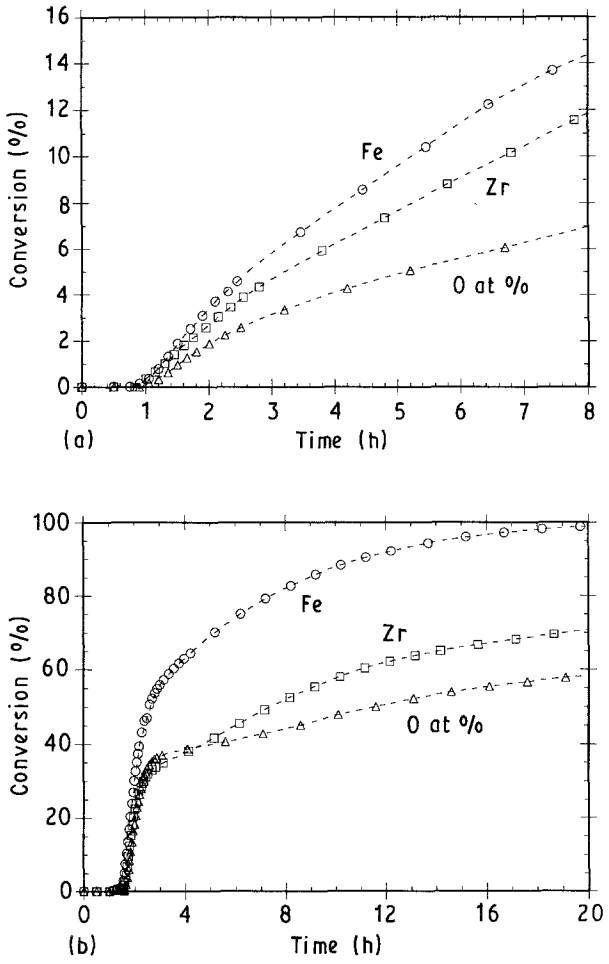

Figure 9 Kinetics for 0.3 at % Fe- and ZrO_2-promoted samples prepared by incipient wetness deposition demonstrating the effect of dissociated nitrogen on the nitridation process, with and without the presence of a transient liquid phase: (a) 1185 °C, (b) 1370 °C. (5–10 μm Si, 50 mg sample size, 5% H_2/N_2, 150 cm^3 min^{-1}).

99% conversion within 20 h, while the zirconium-promoted and 0 at % samples achieved much lower conversions of 71% and 58%, respectively.

Based on Jennings [12], beta-phase production is expected to be enhanced when either atomic nitrogen or liquid phase is present. XRD analysis indeed confirmed this, and indicated α/β phase ratios of 5.1, 4.8, and 3.8 for the unpromoted, zirconium-promoted, and iron-promoted samples, respectively, nitrided at 1370 °C for 25 h. These α/β ratios were determined by modifying the method developed by Gazzara and Messier [69], to enhance the accuracy under conditions where the sample was only *partially* reacted, i.e. when silicon was present in addition to the two phases, α and β [44].

A series of complementary experiments were conducted to elucidate further the effects of dissociated nitrogen and liquid phase. Iron, Cr_2O_3, and CaO impregnated samples, prepared by incipient wetness deposition, were nitrided at 1320 °C, Fig. 10. At a reaction time of 25 h, the 0.30 at % (0.59 wt %) Fe/Si sample, with its silicide liquid phase and atomic nitrogen formation, was characterized by an 87% conversion to Si_3N_4 (results agreeing favourably with Moser *et al.* [25]), while a similar sample with no metal had only a 61% conversion. In the case of 0.30 at % Cr (i.e. 0.81 wt % Cr_2O_3) loading, which was also expected to yield atomic nitrogen (although less efficiently than iron [70]) and lack liquid phase at 1320 °C, nitridation was also enhanced, but not as dramatically as in the iron case. Conversion at 25 h was only 76%. Likewise with 0.30 at % Ca (i.e. 0.60 wt % CaO) impregnation, which readily formed silicate liquid phase but did not contribute to atomic nitrogen formation to any appreciable extent, conversion enhancement was also observed, but to a lesser extent than with either iron or Cr_2O_3 (only 69% in 25 h). These results suggest that both liquid phase and dissociated nitrogen enhance the nitridation process, and moreover, it appears that the formation of active nitrogen may play a more dominant role than the liquid phase, as seen in the comparison between the CaO (liquid/N_2) and Cr_2O_3 (no liquid/N) runs.

Fig. 11 shows the XRD patterns for the unpromoted and three promoted samples. The α/β phase ratios for these samples are summarized in Table III. Also indicated are α/β ratios for the previously described runs at 1370 °C involving zirconium and iron, illustrating the effect of increasing temperature in lowering the ratio, i.e. enhancing β-phase development.

In all the cases at 1320 °C, alpha-phase formation was dominant, especially for the CaO run in which an α/β ratio of approximately 10.2 was observed, Fig. 11a. In comparison, the unpromoted sample yielded an α/β ratio of 7.8, Fig. 11b. This enhancement can be explained by considering the path to equilibrium of the CaO silicide and silicate phases as the sample is heated to reaction temperature. Liquid will initially appear at 760 °C in the calcium-rich areas as a Ca_2Si silicide [67], indicating liquid-phase development well below the reaction temperature studied.

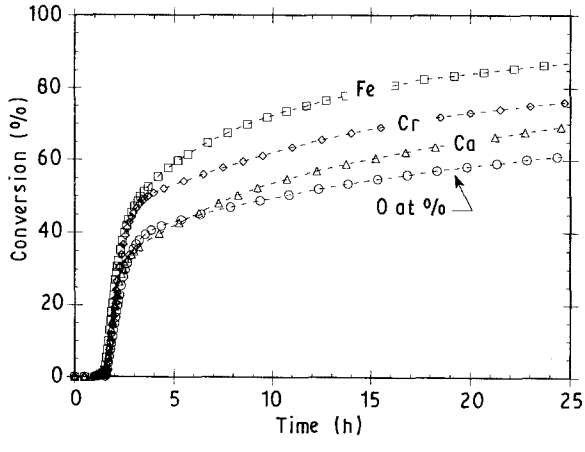

Figure 10 Nitridation kinetics for 0.30 at % Fe-, CaO- and Cr_2O_3-promoted samples prepared by incipient wetness deposition (5–10 μm Si, 50 mg, 1320 °C, 5% H_2/N_2, 150 cm^3 min^{-1}).

TABLE III α/β phase ratios determined by XRD [44] for various metal-prompted (0.3 at %) silicon samples nitrided for 25 h

	O (at %)	Zr	Fe	Cr	Ca
1320 °C	7.8	–	4.8	5.8	10.2
1370 °C	5.1	4.8	3.8	–	–

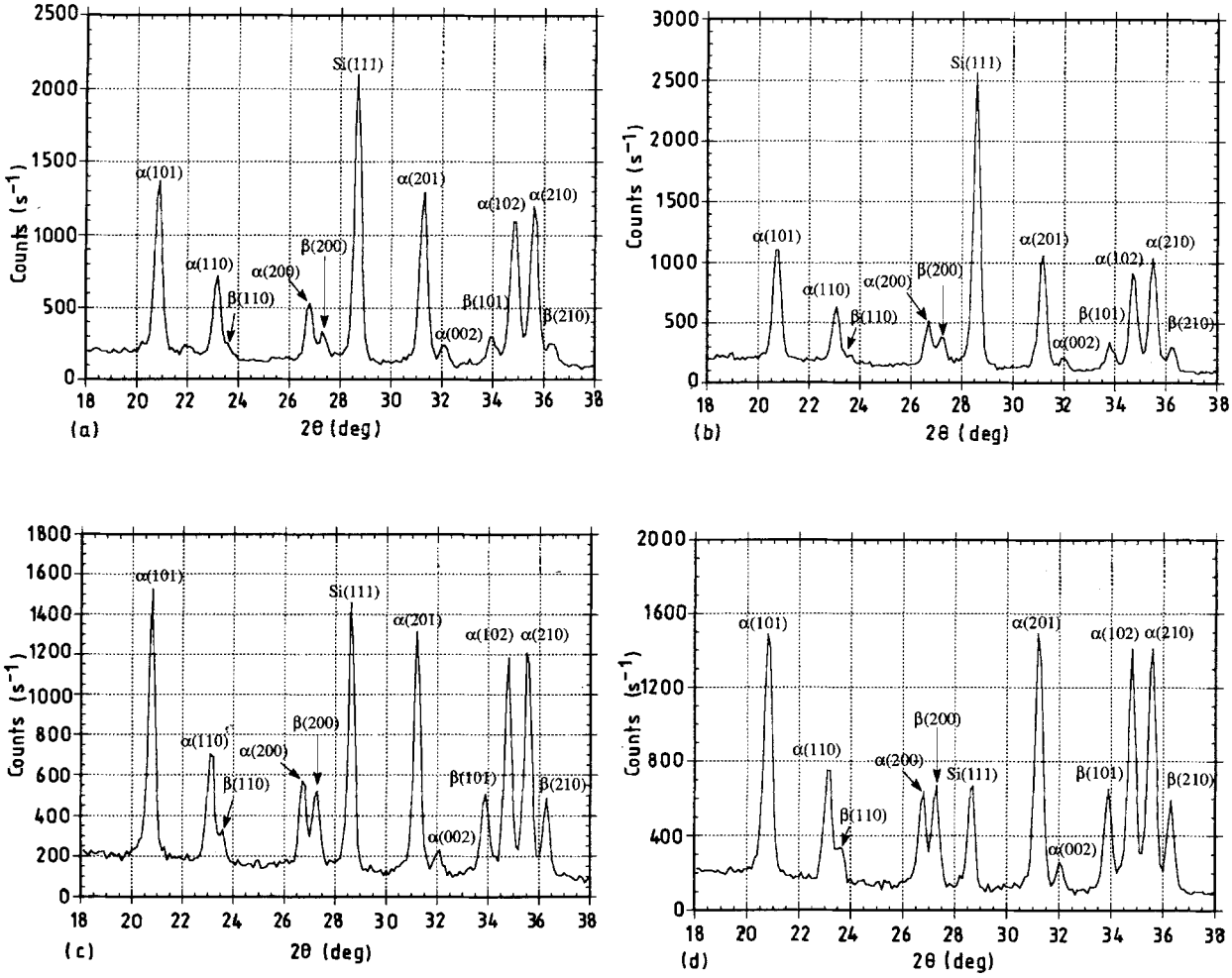

Figure 11 XRD patterns (nickel-filtered CuK_α) for 0.30 at % metal/Si samples after 25 h nitridation time (45 kV, 30 mA, CTHV = 2450, 0.5° 2θ min^{-1}; time constant = 12; slit width = 0.20°). (a) Ca, 69% conversion; (b) no metal, 61% conversion; (c) Cr, 76% conversion; (d) Fe, 87% conversion.

Hence, a liquid phase is present during the majority of the furnace heat-up, most likely resulting in rapid evolution of volatile silicon and SiO at the holding temperature of 1320 °C, and thereby explaining the increased α/β ratio via Reactions 11 and 1 (Table II). For this sample, nitridation initiated at the relatively low temperature of 1065 °C.

$$3Si(g) + 2N_2(g) \rightleftharpoons Si_3N_4(s)$$
$$\Delta G_{1350\,°C} = -851\ kJ\,mol^{-1} \quad (11)$$

The Cr_2O_3- and iron-promoted samples, along with the pure silicon powder, had detectable nitridation initiating at different temperatures, consistent with the nature of the metal additive. As expected, the unpromoted sample started nitriding at the highest temperature (1295 °C), while the metal-promoted samples reacted much earlier during the furnace heat-up (Cr_2O_3 at 1158 °C; iron at 1100 °C). XRD analysis of the metal-promoted samples indicated α/β ratios of 5.8 and 4.8 for Cr_2O_3 (Fig. 11c) and iron (Fig. 11d), respectively. The lower α/β phase ratios for these latter samples can be attributed to the production of atomic nitrogen, which would be expected to have higher diffusivities through the liquid melt (for the iron case) allowing for delivery of the reactant species to the tip of the growing β-crystal consistent with Boyer and Moulson [19], and higher diffusivity through the *c*-axis of the β-crystal (for the Cr_2O_3 case where no liquid was present) consistent with the mechanism of β-Si_3N_4 formation as suggested by Jennings and co-workers [12, 71, 72]. A lower α/β ratio for the iron promoted sample, relative to the Cr_2O_3-promoted sample, likely resulted from the synergistic influence of having both an efficient source of atomic nitrogen in conjunction with the liquid phase. The lower initiation temperatures observed for the Cr_2O_3 and iron samples can be attributed to the enhancement on the initial nucleation process by the presence of atomic nitrogen, following the mechanism proposed by Atkinson *et al.* [65].

The scanning electron micrographs shown in Fig. 12 are representative of the metal-promoted samples. The calcium case yielded a very fine, whisker-like microstructure consistent with a high per cent of α-phase, while the chromium and iron cases tended to form many more interlocking, elongated spikes, characteristic of the β-phase. In addition, the iron-promoted sample suggests nitridation in the presence of liquid phase, possibly involving a solution-precipitation type mechanism.

We are in agreement with Jennings *et al.* [72] in that β-Si_3N_4 formation does not necessarily require liquid phase, although it is indeed favoured by its

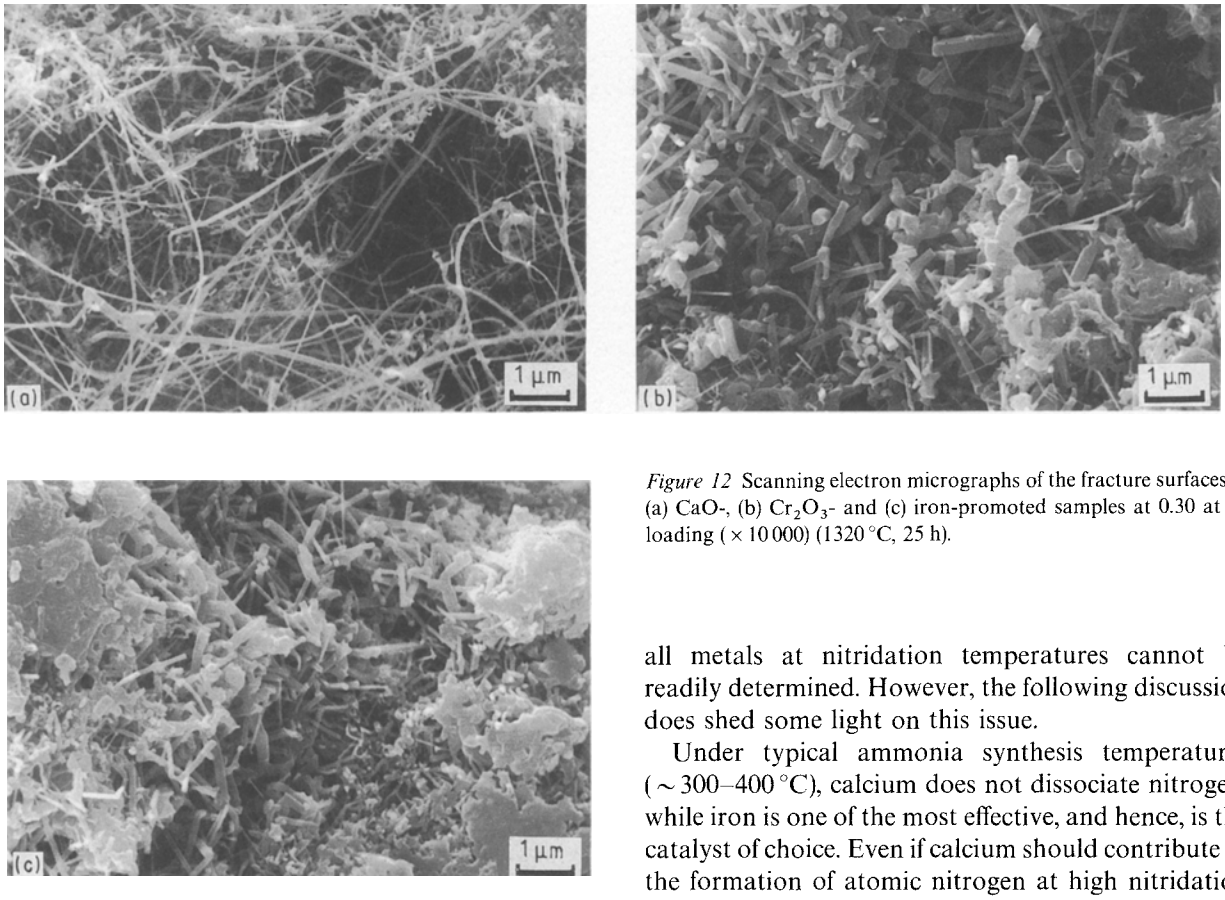

Figure 12 Scanning electron micrographs of the fracture surfaces of (a) CaO-, (b) Cr_2O_3- and (c) iron-promoted samples at 0.30 at % loading (× 10 000) (1320 °C, 25 h).

presence. The liquid provides a rapid diffusion path for nitrogen (especially atomic), and provides the necessary medium for the reconstructive phase transformation that occurs during the densification of RBSN compacts (although not an issue in this paper). Additionally, we have observed that α-phase is stimulated by enhanced volatility of reactant species, Si(g) and SiO(g), when a source of atomic nitrogen is not present.

Obvious caveats to the experiments would include (1) the difficulty in uncoupling the effects of the liquid phase versus the formation of dissociated nitrogen when both are present, (2) the question of similarity between the activity and amount of the various liquid phases, and (3) whether *all* metals dissociate nitrogen at the high temperatures encountered during nitridation. While we do not purport the quantitative aspects of the observed behaviour, we believe that the observations and conclusions are of merit, and that they are applicable to understanding fundamental aspects of the nitridation process and the mechanisms involved.

The first difficulty is effectively addressed by studying the kinetics in the case where there is atomic nitrogen production in the absence of liquid, followed by the combination of the two, and then considering their differences. The main limitation is that higher temperatures are required for the production of liquid phase, and hence, the kinetics observed are partially enhanced by the increased temperature. The second issue of similarity between the activity of the liquid phases is not easily resolved. Likewise, the final concern regarding the production of atomic nitrogen by all metals at nitridation temperatures cannot be readily determined. However, the following discussion does shed some light on this issue.

Under typical ammonia synthesis temperatures (~300–400 °C), calcium does not dissociate nitrogen, while iron is one of the most effective, and hence, is the catalyst of choice. Even if calcium should contribute to the formation of atomic nitrogen at high nitridation temperatures, these experiments do indicate that iron and calcium are distinctly different in their effect on the nitridation rate and conversion, suggesting that iron still retains an edge in its ability to dissociate nitrogen. The differences between iron and calcium cannot be attributed to differences in their ability to disrupt the SiO_2 layer, because these would manifest as variations in the rate during the *initial* stages of nitridation, which in fact were not significant (see Fig. 10). Furthermore, the α/β phase ratios determined by XRD analysis are consistent with the mechanism of Jennings [12], Boyer and Moulson [19], and Atkinson *et al.* [65] which suggest that atomic nitrogen would enhance β-phase formation, while the α-phase likely involves molecular nitrogen. Of course, neither mechanism is expected to be limited to either form of nitrogen. Indeed, experimental evidence clearly indicates that the α-phase involves at least two different mechanisms, one involving the formation of Si_3N_4 nuclei on the silicon surface [65], which would be expected to be enhanced by dissociated chemisorbed nitrogen, and the other involving a vaporization/condensation type mechanism where silicon reacts in the vapour phase and redeposits as α-Si_3N_4, and hence, molecular nitrogen would be pertinent, Reaction 11.

Conditions are favourable for this reaction with a large and negative ΔG^0. The maximum nitridation rates observed experimentally of the order of 10^{-7} kg m^{-2} sec^{-1} [15] could theoretically be maintained by the rate of evaporation of silicon (7.7×10^{-6} kg m^{-2} s^{-1} at 1350 °C, based on Langmuir's equation [73]) due to its high partial pressure at nitridation temperatures (2.6×10^{-9} to 3.0×10^{-7} atm between 1200 and 1400 °C [47]). Furthermore, the nature of

this latter mechanism is consistent with the observed retention of overall external dimensions of the compact.

3.6. Enhancement due to iron at various levels

Some interesting features of the nitridation process are revealed by the impregnation of a range of iron concentrations, Fig. 13a. Clearly, there is an overall enhancement, which can be attributed to the formation of a liquid silicide phase (leading to rapid diffusion paths and Si(g) production) on the surfaces of the silicon grains, and also to the dissociative chemisorption of nitrogen. A dramatic increase in the rate and overall conversion of silicon is observed even at the lowest concentration of iron tested, 0.005 wt %, Fig. 13b. Increasing the iron concentration up to 0.02 wt % results in further enhancement as expected, but as the concentration is increased beyond this level to 0.035 wt %, a decrease in the rate during the early stages of reaction is observed. This decrease may be due to an increase in the thickness of the liquid silicide which the nitrogen must diffuse through in order to reach the silicon core. Evidence has shown [15] that initially there is unhindered diffusion of nitrogen to all internal regions of the compact, regardless of whether the particles are near the outer edge or located near the centre. Hence, we would expect, at least at this early stage in the process, that there is sufficient unreacted or readily available silicon exposed to the nitrogen so that the diffusion enhancement due to the liquid silicide is not realized. In fact, we propose that this melt may be somewhat of a hindrance at this stage, either by decreasing the diffusion of nitrogen or by inhibiting the removal of the SiO_2 layer by its coverage. However, at later stages in the reaction, when the silicon core is not so readily available, the effect of the additional liquid melt becomes apparent. Indeed, a monotonically increasing functional dependence of overall conversion upon weight per cent iron is observed at the later stages of reaction, Fig. 13c.

The enhancement effects of iron appear to make another transition at about 0.6 wt % Fe. Increasing the iron concentration above this value results in an excessive amount of liquid phase on the unreacted surfaces of the silicon particles and also within the interstitial spaces between the particles in the compact. Both microscopic diffusion through the developing product layer and macroscopic binary diffusion between the particles are restricted, causing the rate to be hindered, Fig. 13d. Eventually, however, as the reaction progresses and the compact densifies, through porosity is sealed off, making full conversion in unpromoted samples difficult. The liquid phase then provides the main viable pathway for nitrogen to

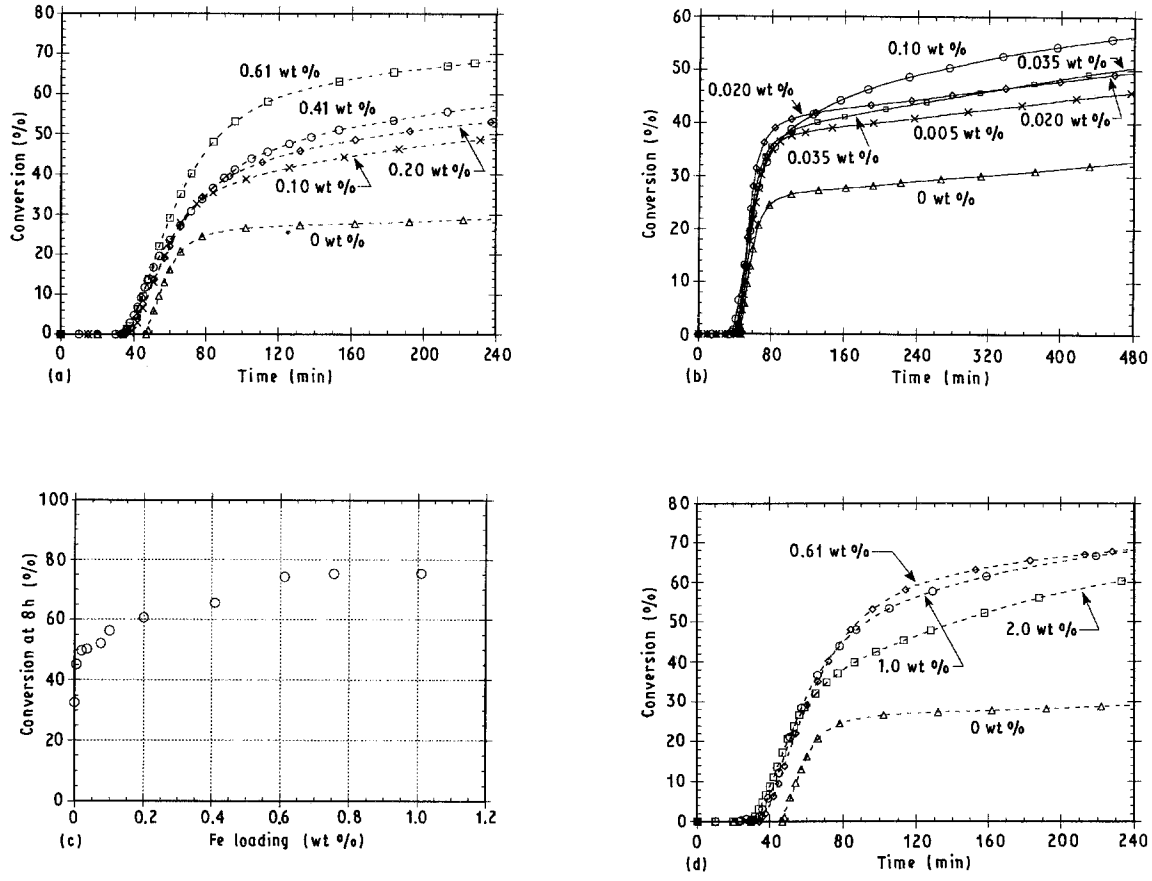

Figure 13 Influence of iron on the nitridation behaviour. (a) Conversion enhancement for silicon powder with iron deposition at various levels prepared by incipient wetness deposition. (b) Influence of low levels of iron addition on early conversion showing a transition between the 0.020 and 0.035 wt % runs. (c) Overall conversion to silicon nitride at 8 h reaction time. (d) Effect of excess liquid-phase formation on the early stages of the nitridation kinetics. (– 325 mesh Si, 100 mg sample size, 1350 °C, 5% H_2/N_2, 150 cm^3 min^{-1}).

reach the unreacted silicon, eventually yielding overall conversions that are higher for the greater iron loadings (at least up to 2.0 wt% Fe).

4. Conclusions

(1) Both mullite and high-purity alumina tubes typically used in nitridation experiments are limitless reservoirs for contamination impurities at reaction temperatures. The SiO(g) generated can react directly, or decompose and subsequently deposit as Si(s) and cristobalite SiO_2(s), which in turn can also react to form Si_3N_4. α-phase is the likely product. The metallic constituents emitted from the oxide tubes, such as aluminium, iron and potassium, likely affect the course of reaction, as was shown for metals deliberately added to the samples.

(2) The pertinent reactions affecting the SiO(g) equilibria during the nitridation process are summarized in Table II. SiO nitridation is thermodynamically feasible under typical "high-purity" (10^{-6} atm O_2 and H_2O) reaction conditions in spite of the adverse thermodynamics (Reaction 1). The presence of 5% H_2 markedly enhances the observed kinetics by aiding the removal of oxygen from the reaction zone (Reaction 6). The expected enhancement in SiO(g) production through the devitrification of SiO_2(s) (Reaction 7), resulting from the addition of 5% H_2, is negligible. That is, SiO(g) production remains about the same as in the 0% H_2 case. This is a result of the additional H_2O(g) produced in the presence of the added hydrogen (Reaction 5), thereby shifting Reaction 7 equilibrium to the left. However, both Reactions 4 and 7 are the primary sources of SiO(g) during nitridation, with a minor contribution resulting from the active oxidation of Si(s) (Reaction 2).

(3) Pre-sintering of silicon compacts prior to nitridation alters the pore size and distribution unfavourably. Nitridation rates are reduced as the sintering time is increased. Achieving full conversion is markedly impeded.

(4) Quantitative kinetic analysis of nitridation data requires intrinsic effects to be isolated from those amenable to the global scale. The vast majority of existing data in the nitridation literature is applicable only to a specific set of conditions, i.e. the experimental conditions in which the data were obtained, making quantitative analysis difficult. Compact effects are likely the most significant factor in rendering data specific for a given nitridation system, followed closely by particle shape and size distribution. These issues have recently been addressed [15].

(5) β-Si_3N_4 production is not strictly limited to the presence of liquid phases as was previously postulated [19], and furthermore, is not necessarily stimulated by the presence of liquid phase as was shown in the calcium promoted run in which a high α/β ratio resulted (10.2/1).

(6) Atomic nitrogen may indeed be a factor in enhancing the formation of the β-phase, as postulated by Jennings [12]. This was demonstrated by the lower α/β ratio (5.8/1) observed in the Cr_2O_3-promoted run, in which atomic nitrogen was produced in the absence of liquid phase. This is in comparison to the unpromoted sample which had an α/β ratio of 7.8/1, where neither atomic nitrogen nor liquid phase was present.

(7) Liquid phases are significant contributors to the production of silicon vapour. This vapour reacts to form α-Si_3N_4 through a vaporization/condensation type mechanism given by Reaction 11, and appears to be the dominant mode of α-phase production when liquid phases are present.

(8) Iron markedly enhances the rate and overall conversion of Si(s) → Si_3N_4(s) by (1) catalysing the production of atomic nitrogen (promoting β-phase development), (2) forming liquid phases which provide rapid diffusion paths and a source of volatile silicon, and (3) by aiding devitrification of SiO_2(s) which provides an additional source of SiO(g) and exposes underlying silicon to the reactant gas.

Acknowledgement

One of the authors (R.G.P.) gratefully acknowledges the award of a Graduate Assistance in the Area of National Needs (GAANN) Fellowship, under the auspices of the Center for Bioengineering and Pollution Control at the University of Notre Dame, during the course of this study.

References

1. G. ZIEGLER, J. HEINRICH and G. WÖTTING, *J. Mater. Sci.* **22** (1987) 3041.
2. A. ATKINSON, P. J. LEATT and A. J. MOULSON, *Proc. Brit. Ceram. Soc.* **22** (1973) 253.
3. A. GIACHELLO and P. POPPER, *Ceram. Int.* **5** (1979) 110.
4. J. A. MANGELS and G. J. TENNENHOUSE, *Bull. Amer. Ceram. Soc.* **60** (1981) 1306.
5. G. K. WATSON, T. J. MOORE and M. L. MILLARD, *J. Amer. Ceram. Soc.* **67** (1984) C-208.
6. D. M. MIESKOWSKI and W. A. SANDERS, *ibid.* **68** (1985) C-217.
7. L. K. L. FALK, R. POMPE and G. L. DUNLOP, *J. Mater. Sci.* **20** (1985) 3545.
8. W. HERMEL, M. HERRMANN, J. PABST and R. SCHOBER, in "Sintering '87", Vol. 2, edited by S. Somiya, M. Shimada, M. Yoshimura and R. Wantanabe (Elsevier Applied Science, New York, 1988) p. 998.
9. M. HERRMANN, S. HESS, H. KESSLER, J. PABST and W. HERMEL, in "Science of Sintering", edited by D. P. Uskokovic, H. Palmour III and R.M. Spriggs (Plenum Press, New York, 1989) p. 421.
10. C. GRESKOVICH and J. H. ROSOLOWSKI, *J. Amer. Ceram. Soc.* **59** (1976) 336.
11. A. J. MOULSON, *J. Mater. Sci.* **14** (1979) 1017.
12. H. M. JENNINGS, *ibid.* **18** (1983) 951.
13. J. A. MANGELS, *Bull. Amer. Ceram. Soc.* **60** (1981) 613.
14. P. WONG and D. R. MESSIER, *ibid.* **57** (1978) 525.
15. R. G. PIGEON and A. VARMA, *J. Mater. Sci.* (1993) in press.
16. M. MITOMO, *ibid.* **12** (1977) 273.
17. S.-S. LIN, *J. Amer. Ceram. Soc.* **60** (1977) 78.
18. *Idem, ibid.* **61** (1978) 95.
19. S. M. BOYER and A. J. MOULSON, *J. Mater. Sci.* **13** (1978) 1637.
20. W. A. FATE and M. E. MILBERG, *J. Amer. Ceram. Soc.* **61** (1978) 531.
21. D. CAMPOS-LORIZ, S. P. HOWLETT, F. L. RILEY and F. YUSAF, *J. Mater. Sci.* **14** (1979) 2325.
22. J. MUKERJI and S. K. BISWAS, *J. Amer. Ceram. Soc.* **64** (1981) 549.

23. J. R. G. EVANS and A. J. MOULSON, *J. Mater. Sci.* **18** (1983) 3721.
24. C. E. BOULDIN, E. A. STERN, M. S. DONLEY and T. G. STOEBE, *ibid.* **20** (1985) 1807.
25. W. R. MOSER, D. S. BRIERE, R. CORREIA and G. A. ROSSETTI, *J. Mater. Res.* **1** (1986) 797.
26. R. B. GUTHRIE and F. L. RILEY, *J. Mater. Sci. Lett.* **9** (1974) 1363.
27. D. CAMPOS-LORIZ and F.L. RILEY, *ibid.* **11** (1976) 195.
28. J. A. MANGELS, *J. Amer. Ceram. Soc.* **58** (1975) 354.
29. D. P. ELIAS and M. W. LINDLEY, *J. Mater. Sci.* **11** (1976) 1278.
30. B. F. JONES and M. W. LINDLEY, *J. Mat. Sci. Lett.* **11** (1976) 1969.
31. W. M. DAWSON and A. J. MOULSON, *ibid.* **13** (1978) 2289.
32. M. W. LINDLEY, D. P. ELIAS, B. F. JONES and K. C. PITMAN, *J. Mater. Sci.* **14** (1979) 70.
33. D. CAMPOS-LORIZ and F.L. RILEY, *J. Mat. Sci. Lett.* **14** (1979) 1007.
34. H. DERVISBEGOVIC and F. L. RILEY, *ibid.* **14** (1979) 1265.
35. *Idem, J. Mater. Sci.* **16** (1981) 1945.
36. N. J. SHAW, *J. Mater. Sci. Lett.* **1** (1982) 337.
37. H. KIM and C. H. KIM, *ibid.* **3** (1984) 199.
38. *Idem, ibid.* **3** (1984) 201.
39. *Idem, ibid.* **3** (1984) 203.
40. *Idem, J. Mat. Sci.* **20** (1985) 141.
41. *Idem, ibid.* **20** (1985) 149.
42. M. N. RAHAMAN and A. J. MOULSON, *ibid.* **19** (1984) 189.
43. B. F. JONES and M. W. LINDLEY, *ibid.* **11** (1976) 1288.
44. R. G. PIGEON and A. VARMA, *J. Mater. Sci. Lett.* **11** (1992) 1370.
45. D. H. FILSINGER and D. B. BOURRIE, *J. Amer. Ceram. Soc.* **73** (1990) 1726.
46. F. L. RILEY, *Mater. Sci. Forum* **47** (1989) 70.
47. C. L. YAWS, L. L. DICKENS, R. LUTWACK and G. HSU, *Solid State Tech.* January (1981) 87.
48. O. J. WHITTEMORE Jr, in "Proceedings of the 14th University Conference on Ceramic Science", Vol. 11, edited by H. Palmour III, R. F. Davis and T. M. Hare (Plenum Press, New York, 1978) p. 125.
49. G. L. MESSING, C. J. MARKHOFF and L. G. McCOY, *Bull. Amer. Ceram. Soc.* **61** (1982) 857.
50. J. ZHAO and M. P. HARMER, *J. Amer. Ceram. Soc.* **71** (1988) 113.
51. *Idem, ibid.* **71** (1988) 530.
52. E. C. M. PENNINGS and W. GRELINER, *ibid.* **72** (1989) 1268.
53. J. ZHENG and J. S. REED, *ibid.* **72** (1989) 810.
54. J. ZHENG, P. F. JOHNSON and J. S. REED, *ibid.* **73** (1990) 1392.
55. N. NAITO, L. C. JONGHE and M. N. RAHAMAN, *J. Mater. Sci.* **25** (1990) 1686.
56. B. F. JONES and M. W. LINDLEY, *J. Mater. Sci. Lett.* **12** (1977) 630.
57. S. C. DANFORTH, H. M. JENNINGS and M. H. RICHMAN, *ibid.* **13** (1978) 1590.
58. S. C. DANFORTH and M. H. RICHMAN, *ibid.* **14** (1979) 240.
59. B. F. JONES and M. W. LINDLEY, *ibid.* **11** (1976) 191.
60. G. F. FROMENT and K. B. BISCHOFF, "Chemical Reactor Analysis and Design", 2nd Edn (Wiley, New York, 1990) p. 142.
61. P. ARUNDALE and A. J. MOUSLON, *J. Mater. Sci. Lett.* **12** (1977) 2138.
62. W. S. COBLENZ, *J. Mater. Sci.* **25** (1990) 2754.
63. W. M. ROBERTSON, *J. Amer. Ceram. Soc.* **64** (1981) 9.
64. F. W. AINGER, *J. Mater. Sci.* **1** (1966) 1.
65. A. ATKINSON, A. J. MOULSON and E. W. ROBERTS, *J. Amer. Ceram. Soc.* **59** (1976) 285.
66. H. M. JENNINGS, *J. Mater. Res.* **3** (1988) 907.
67. F. N. RHINES, "Phase Diagrams in Metallurgy: Their Development and Application" (McGraw-Hill, New York, 1956).
68. A. S. BEREZHNOI, "Silicon and Its Binary Systems" (Consultants Bureau, New York, 1960).
69. C. P. GAZZARA and D. R. MESSIER, *Bull. Amer. Ceram. Soc.* **56** (1977) 777.
70. G. C. BOND, "Heterogeneous Catalysis: Principles and Applications" (Oxford University Press, London, 1974) p. 28.
71. H. M. JENNINGS and M. H. RICHMAN, *J. Mater. Sci.* **11** (1976) 2087.
72. H. M. JENNINGS, S. C. DANFORTH and M. H. RICHMAN, *J. Mater. Sci. Lett.* **14** (1979) 1013.
73. I. LANGMUIR, *Phys. Rev.* **5** (II) (1913) 329.

Received 4 March and accepted 25 June 1992